Journal of Sound and Vibration (2000) **231**(3), 563–575
doi:10.1006/jsvi.1999.2545, available online at http://www.idealibrary.com on IDEAL®

AEROACOUSTICAL STUDY OF THE TGV PANTOGRAPH RECESS

C. NOGER, J. C. PATRAT, J. PEUBE AND J. L. PEUBE

Laboratoire d'Etudes Aérodynamiques-CEAT-UMR CNRS 6609, 43, *Rue de l'Aérodrome*, 86036 *Poitiers Cedex*, *France*

(*Received in final form* 23 *September* 1999)

The general focus of this aerodynamic noise research, induced by turbulent incompressible flow, is to improve our knowledge of acoustic production mechanisms in the TGV pantograph recess in order to be able to reduce the radiated noise. This work is performed under contract with SNCF as a part of the German–French Cooperation *DEUFRAKO K2*, and is supported by French Ministries for Transport and Research. Previous studies on TGV noise source locations (*DEUFRAKO K*) have identified the pantograph recess as one of the important aerodynamic noise sources, for speeds higher than 300 km/h, due to flow separation. The pantograph recess is a very complex rectangular cavity, located both on the power car and the first coach roofs of the TGV, and has not been studied before due to the complex shapes. Its aeroacoustic features are investigated experimentally in a low-subsonic wind tunnel, on a realistic 1/7th scale mock-up both with and without pantographs. Flow velocities, estimated with hot-wire anemometry, and parietal visualizations show the flow to reattach on the recess bottom wall and to separate again at the downstream face. Wall pressure fluctuations and "acoustic" measurements using $\frac{1}{4}$ and $\frac{1}{2}$ in microphones respectively are also measured to qualify the flow: no aerodynamic or acoustic oscillations are observed. The study indicates that the pantograph recess has a different behaviour compared to the usual cavity grazing flows.

1. INTRODUCTION

Aerodynamic sound can occur under various circumstances including regions of flow separation, which occur on the TGV roof in the pantograph recess. The pantograph recess is an extremely complex cavity located both on the power car and the first coach of the TGV and is composed of several elements (see terminology in Figure 1).

Cavity grazing flows are of interest because, under certain conditions, they can lead to the development of high-pressure oscillations due to non-linear couplings (self-sustained oscillations) thus involving aerodynamic noise and drag, fatigue ruptures or significant noise generation. Although numerous of studies have been carried out recently on cavity grazing flows (theoretical [1–3], experimental [4–11] or numerical [10, 12, 13]) over a wide range of Mach and Reynolds numbers with both laminar and turbulent boundary layers and over various length-to-depth

0022-460X/00/130563 + 13 $35.00/0

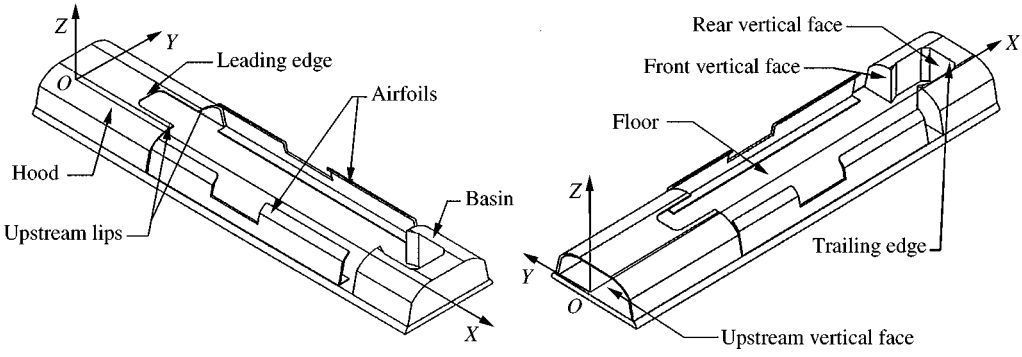

Figure 1. Terminology of the pantograph recess.

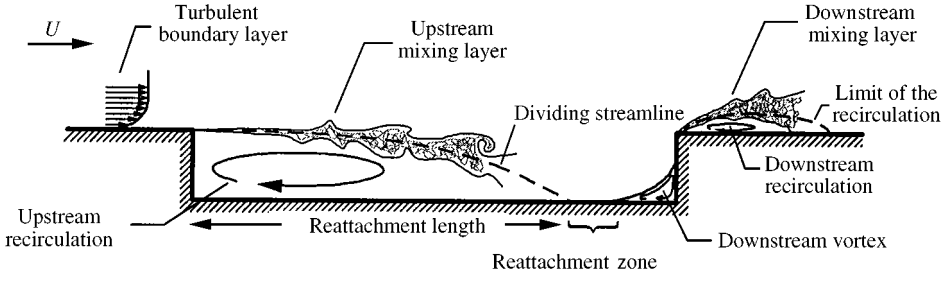

Figure 2. Features of a closed cavity grazing flow.

ratios (L/D), relatively few studies have dealt with the pantograph recess whose geometry (length L, depth D and width W) gives ratios of $L/D > 7{\cdot}4$ to $10{\cdot}2$ and $L/W > 2{\cdot}5$ to $3{\cdot}5$. Its characteristics imply that it can be qualified as a closed ($L/D > 7$–8 [4, 6]), three-dimensional ($L/W > 1$ [11]) cavity. This classification already allows a short description of the flow structure that may occur inside the recess to be given. The upstream boundary layer separates at the leading edge, involving a turbulent zone (with high mean velocity gradients), transforms into a shear layer profile and reattaches on the cavity floor (bottom wall). Just in front of the rear vertical face, the flow separates again, giving rise to a vortex corner. Downstream from the trailing edge, a second recirculation, particularly influenced by the flow structure inside the cavity, develops due to a strong separation of the flow (Figure 2).

The pantograph recess features are investigated experimentally both from aerodynamic and acoustic points of view at low subsonic speeds. The investigations include two different studies concerning two different mock-up configurations.

2. EXPERIMENTAL APPARATUS

Wind tunnel—Experiments were conducted in the low-subsonic Nieuport wind tunnel of the *LEA* at Poitiers from speeds of a few meters per second up to

a maximum free-stream velocity of 38 m/s. The test section is about 1·7 m diameter and 2·4 m long.

TGV mock-up—The 1/7th scale mock-up is about 10 m long and 0·55 m high. The pantograph recess (about 1·5 m long and 0·1 m high) is essentially composed of four elements: an upstream hood, two aerofoils and a downstream basin (Figure 1). During the first study, a simple upstream hood was used to obtain the initial results of the flow structure inside the recess, whereas during the second, a hood with fences is used and the pantographs are taken into account.

Aerodynamics—Both the velocities and the turbulence intensities are measured using hot-wire anemometry (constant temperature hot-wire anemometry, CTA) upstream, inside and downstream of the pantograph recess. Different transverse positions were measured but only results relating to the recess centreline are discussed here.

Acoustics—A $\frac{1}{2}$ in electrostatic microphone equipped with a nose cone was used to make "acoustic" measurement along the recess centreline. Wall pressure fluctuations were measured along the pantograph recess with $\frac{1}{4}$ in electrostatic microphones mounted at grazing incidence.

For practical reasons, results of visualizations, hot-wire or microphone measurements of the two different studies are always presented or plotted together.

3. FIRST MEASUREMENT STUDY

Following the very complex geometry of the pantograph recess (Figure 3), the first study began with parietal flow visualizations to study the details of the flow inside and around the recess. It was completed by dual-component velocity measurements, "acoustic" measurements and finally wall pressure fluctuation measurements.

3.1. PARIETAL FLOW VISUALIZATIONS

The visualizations were obtained by mixing kaolin with kerosene and painting the walls uniformly with this mixture. When the kerosene has evaporated the wind tunnel is turned off. Figure 4 shows the hood and basin top view visualizations: the flow goes from the left to the right of the photographs. As indicated by the

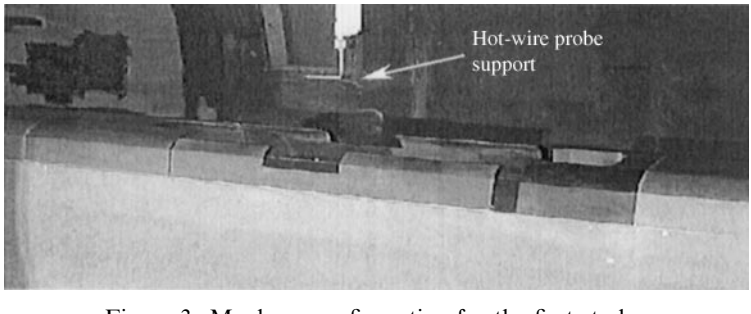

Figure 3. Mock-up configuration for the first study.

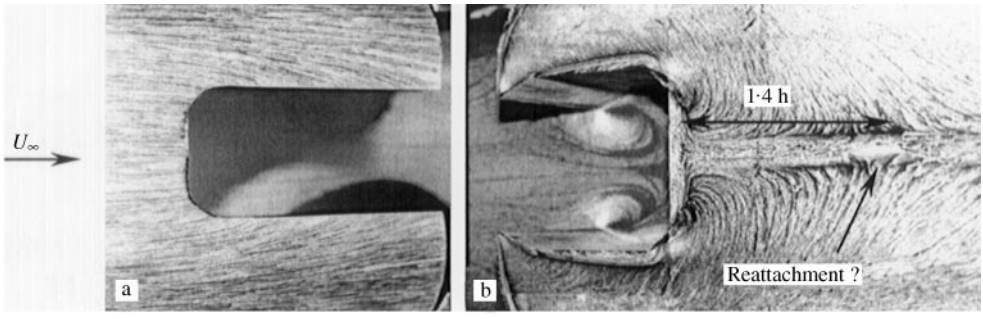

Figure 4. Top views of the hood and basin visualisations of the first study.

streamline curvatures (Figure 4(a)), the flow is attracted towards the hood fence (with relatively good symmetry). Because of the "*U*" shaped hood the upstream turbulent boundary layer separates at different streamwise locations from the hood extremity. The flow inside the recess is too turbulent to obtain accurate information about the different impingement locations and has a tendency to be carried towards the aerofoils after its impingement on the floor. Nevertheless, at the basin downstream, several vortex locations can be observed just in front of its front and rear vertical faces and downstream of the trailing edge (Figure 4(b)). Two symmetrical intensive contra-rotating vortices are created due to the interaction of the flow separation with the sharp edges (in front of the rear face), followed by a downstream "reattachment" point. Moreover, the flow undergoes an important acceleration when entering the basin due to the section contraction and the two sharp edges create spool vortices that impinge on the basin downstream vertical face. Just behind the trailing edge, one can note the presence of several other small vortices nesting near the basin corners, which make this flow structure very complex.

From these results, the reattachment and separation lengths along the centreline can be deduced. The oncoming turbulent boundary layer separates from the hood leading edge and impinges about $3h$ from the leading edge (h being the step height), separates again $0{\cdot}7h$ in front of the rear vertical face and finally "impinges" $1{\cdot}4h$ downstream of the trailing edge. This last point is more difficult to interpret: it seems that there is no reattachment point but rather a recirculation created by the fluid aspiration, due to a strong vertical jet developing at the trailing edge which provokes the flow to move towards the upstream. This is different from normal cavity or rearward facing step results.

3.2. VELOCITY MEASUREMENTS

Constant temperature hot-wire anemometry (CTA) is used to measure both the longitudinal and vertical fluctuations. The recess centreline characteristics (Figures 5(a), 6(a) and 7(a)) for a free-stream velocity of 37 m/s show that the oncoming boundary layer is fully turbulent ($Re_x = 8{\cdot}4 \times 10^6$). As expected and confirmed by the visualizations, the upstream boundary layer transforms into

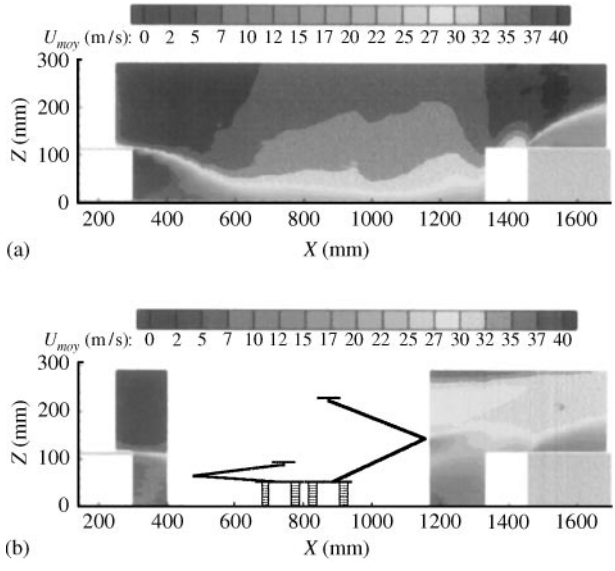

Figure 5. Longitudinal velocity in the recess centreline: first (a) and second (b) configurations.

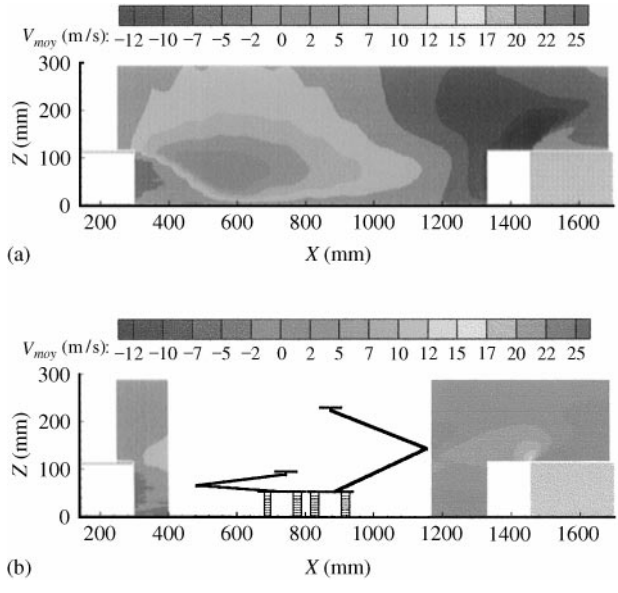

Figure 6. Vertical velocity in the recess centreline: first (a) and second (b) configurations.

a shear layer and impinges on the floor about 3h from the hood leading edge. The blank areas on the figures correspond to regions where hot-wire anemometry is not well suited to the accurate determination of velocities and turbulence, or where measurements cannot be made with the hot-wire probe support. The longitudinal velocity shown in Figure 5(a) indicate that the upstream shear layer curves sharply and soon impinges on the floor when compared to normal cavity flows (about 5h to 7h [4]); this is due to important three-dimensional effects developing both at the

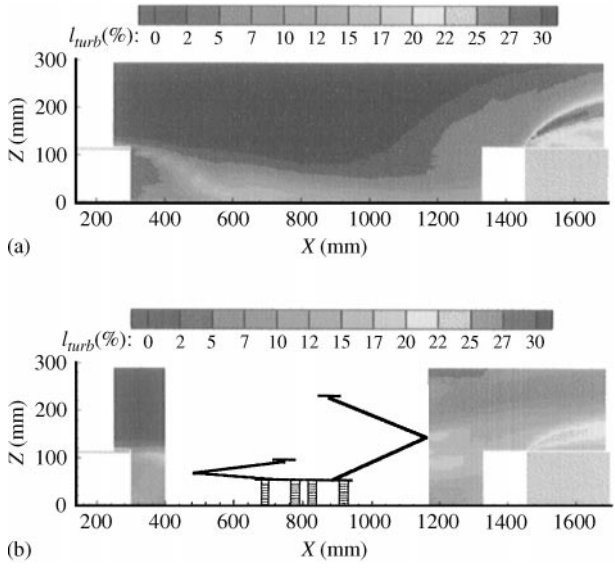

Figure 7. Turbulence intensity in the recess centreline: first (a) and second (b) configurations.

hood leading edge and upstream lips which are responsible for streamwise vortex appearances. The downstream "reattachment" point is always difficult to interpret, the region being too three-dimensional and because negative longitudinal velocities cannot be measured with the hot-wire technique. The vertical velocity diagram (Figure 6(a)) does not help to clarify the issue but shows the strong vertical jet developing at the trailing edge (about 45° inclined).

The turbulence intensity contours (approximated with $I_{turb}^{mes} = \sqrt{\overline{u^2} + \overline{v^2}}/U_\infty$ in Figure 7(a)) distinguish between shear layer and free-stream zones; the first mixing layer reaches a value of around 20%, whereas the downstream layer is most intense and reaches 30% at the basin trailing edge. One can again notice the sharp curvature of the oncoming shear layer. When distinguishing between longitudinal and vertical turbulence intensities, it indicates that the longitudinal dominates in the generation of turbulence. Away from the centreline [14], the upstream shear layer dives very sharply, the flow becomes more and more turbulent inside (30%) and downstream from the recess (50%) until encountering the aerofoils, and the impingement length increases in the streamwise direction.

3.3. PRESSURE MEASUREMENTS

The pressure measurements consisted of both "acoustic" and wall pressure fluctuation measurements. These were carried out with a $\frac{1}{2}$ in microphone placed on the centreline above the recess (285 mm) and with $\frac{1}{4}$ in microphones mounted at grazing incidence.

3.3.1. "*Acoustic*" *measurements*

The $\frac{1}{2}$ in microphone was equipped with a nose cone and installed in place of the hot wire on the same support, parallel to the free-stream velocity on the recess

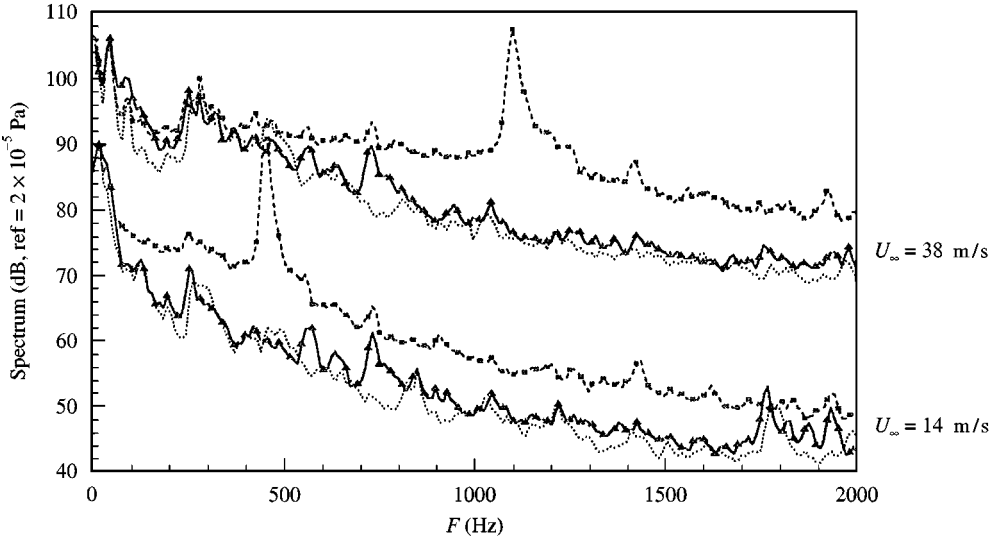

Figure 8. "Acoustic" measurement in the recess centreline ($x = 1150$ mm). · · · · · · ·, reference without cavity; –▲–, 1st campaign with cavity; - - - -■- - - -, 2nd campaign with fences and pantos.

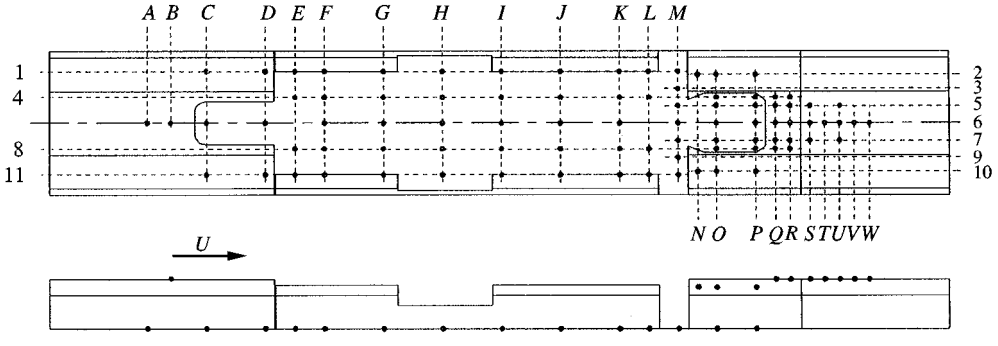

Figure 9. Wall pressure fluctuation locations.

centreline. Figure 8 shows the spectral content of the radiated noise for the two different studies and for two free-stream velocities, at a position of 1150 mm from the upstream vertical face. It is possible to distinguish between aerodynamic/acoustic sources and the pantograph recess contribution to the overall noise; the spectrum with the cavity (solid line) is approximately 2 dB higher than the one without the cavity (dotted line) for the different speeds.

3.3.2. *Wall pressure fluctuations* (*w.p.f.*)

Eighty-eight pressure holes were distributed along the recess streamwise and spanwise (Figure 9). All the wall pressure fluctuations (w.p.f.) were measured at the maximum free-stream velocity (38 m/s). The study of the different pressure locations shows two regions of interest. The first, located under the upstream hood, is composed of resonant frequencies that are not velocity dependent (acoustic origin). The frequency peaks in the spectrum vary with streamwise (Figure 10(a)) and spanwise locations indicating pressure nodes and anti-nodes.

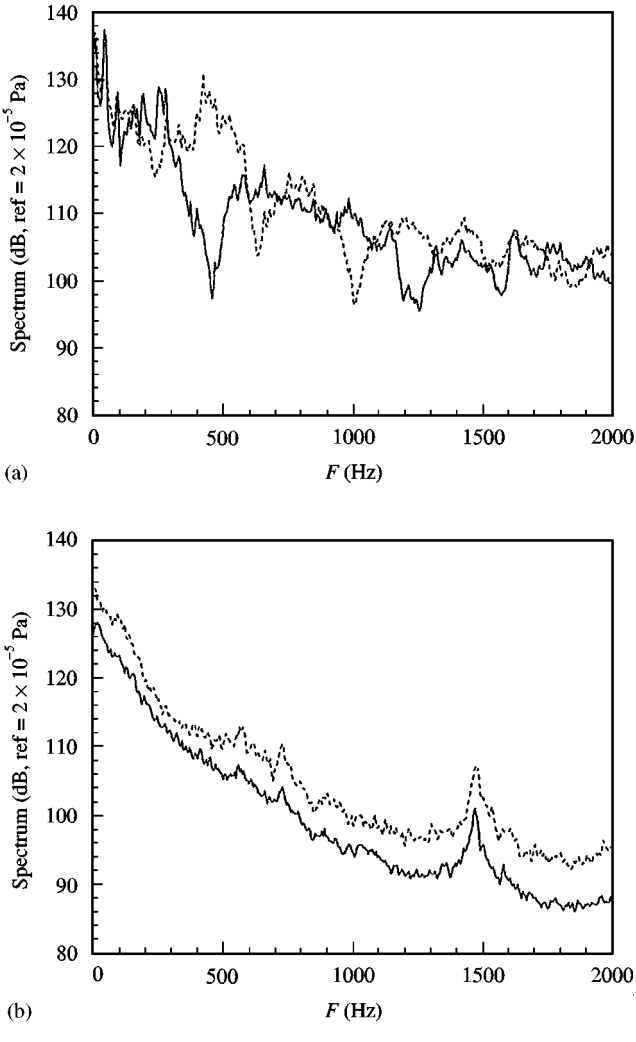

Figure 10. Hood (a) and basin (b) wall pressure fluctuation features of the first study. ———, micro a6, micro o4; - - - - - -, micro d6, micro p4.

The second region corresponds to the basin interior (Figure 10(b)) which is excited by the flow at a resonant frequency of approximately 1475 Hz corresponding to a basin transverse mode. The other pantograph recess spectra look like ordinary attached turbulent flow spectra (most of the energy being concentrated in the low-frequency range) and do not contain any peaks which could confirm the presence of oscillations.

The root-mean-square (r.m.s.) pressure coefficients $C_{P_{r.m.s.}}$ (estimated with $C_{P_{r.m.s.}} = P_{r.m.s.}/\frac{1}{2}\rho U_\infty^2$ at each microphone location) identify several regions (Figure 11). Note that the configuration is not perfectly symmetrical although the visualizations are. The upstream shear layer impingement on the recess floor could be expected to give a high pressure level (0·22) but there is nothing significant at the trailing edge compared with the usual cavity pressure coefficients, which give a maximum just downstream from the trailing edge [7]. This is partly explained by

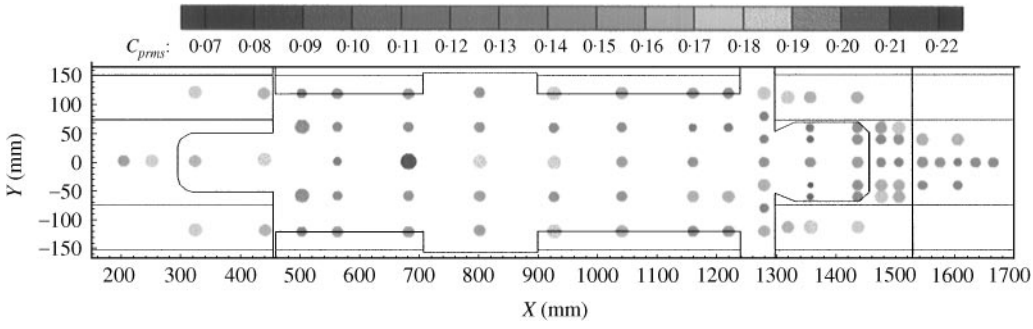

Figure 11. Root-mean-square pressure coefficient ($C_{P_{r.m.s}}$) recess without pantograph.

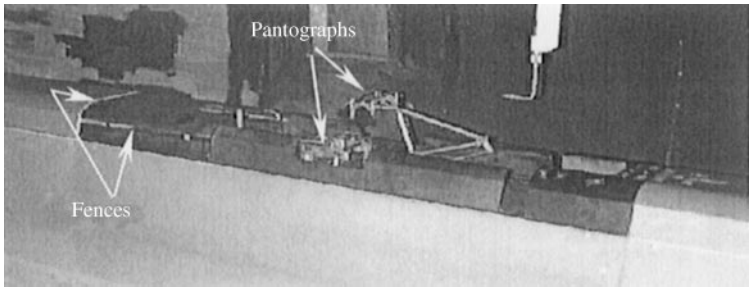

Figure 12. Mock-up configuration of the second study.

the different behaviour of the recess and by the fact that there is no reattachment. The downstream shear layer development is not the only source of high pressures but one of the elements contributing to these high levels. The high-pressure coefficient values are explained by the presence of many three-dimensional effects.

Coherence between w.p.f. and velocity fluctuations downstream from the trailing edge [14] indicates the low frequency aspect of the w.p.f.; that the vertical velocity fluctuations are the most influential on the w.p.f. (55%); and that the w.p.f. are directly dependent on the turbulence restrained around a volume close to the microphones. The maximum of coherence corresponds to the maximum of Reynolds stresses in the downstream shear layer.

4. SECOND MEASUREMENT STUDY (WITH MODIFIED RECESS)

This second study follows the same principle as the first. In this configuration, an upstream hood with fences is used and the two pantographs are taken into account (Figure 12).

4.1. PARIETAL FLOW VISUALIZATIONS

As in the first study, similar visualization characteristics are obtained, the only difference being a slight asymmetry of the flow at the basin entrance due to the

asymmetric configuration of the pantograph locations. Nevertheless, although the reattachment length has increased inside the recess (about 3·7h from the hood leading edge) due to the fence inflow, the downstream features remain approximately the same, the flow separation occurring near 0·7h from the rear vertical face and "impinging" 1·3h downstream the trailing edge.

4.2. VELOCITY MEASUREMENTS

The pantographs do not allow hot-wire probe measurements to be made inside the recess. Nevertheless, exploring the trailing edge region (Figures 5(b), 6(b) and 7(b)) reveals the pantograph wakes (far downstream, inside and above the recess) interacting with the downstream shear layer. The latter is less intensive (25%) than the one in the first study (30%). In fact, the upstream shear layer impinges directly on the first pantograph (rather than the floor) thus increasing the turbulence level inside the recess by more than 10%. It is carried out towards the trailing edge and fills the entire recess interior. The hood side fences provoke a mass inflow which leads to an increase in the first recirculation and causes the flow to be carried downstream with a smaller longitudinal velocity (Figure 5(b)) thus reducing the vertical velocity. Figure 6(b) shows that the downstream vertical jet is reduced both in size and intensity because of the flow impingement upon the downstream vertical face at a higher ordinate.

4.3. PRESSURE MEASUREMENTS

To complete this study, pressure measurements were made with $\frac{1}{2}$ and $\frac{1}{4}$ in microphones to measure both the "acoustic" fluctuations along the recess centreline and the wall pressure fluctuations inside and around the recess (as in the first study).

4.3.1. "*Acoustic*" *measurement*

The addition of fences to the hood decreases the broadband noise level slightly and shifts some recess modes (not shown [14]). On the other hand, the noise of the pantographs dominates the slit effects and generates a high discrete peak (dashed line, Figure 8) corresponding to the Strouhal frequency of one of the predominant perpendicular tubes (i.e., the bow) which constitute them (with regard to the flow direction). When varying the free-stream velocity, the frequency of this peak varies indicating an aerodynamic origin, corresponding to the pantograph vortex shedding (unsteady lift of the tube). This frequency radiates acoustic energy in front of, above and downstream of the recess. An increase of the background noise of about 5–10 dB should also be noted.

4.3.2. *Wall pressure fluctuations*

This configuration has completely modified the spectra both under the hood and in the basin regions. The background noise level (Figure 13(a)) as well as the node and anti-node magnitudes have decreased, when compared with Figure 10(a). This

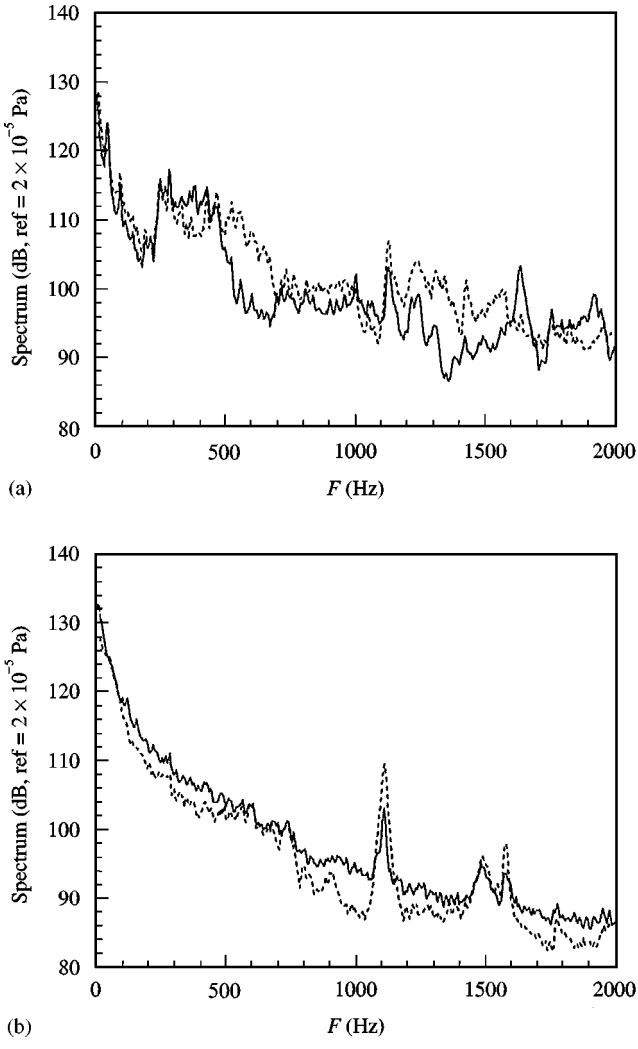

Figure 13. Hood (a) and basin (b) wall pressure fluctuation features of the second study. ———, micro a6, micro o4; ------, micro d6, micro p4.

is due to the hood fence inflow that has encouraged a smoothing of the flow under the hood. The pantograph peak influences the microphones located under the hood but does not interact with the basin frequency resonant mode (Figure 10(b)).

The r.m.s. pressure coefficients $C_{P_{r.m.s.}}$ allow several regions to be identified (Figure 14). The overall coefficients levels are lower than those of the first configuration; the maximum reaches approximately 0·18 and all the levels are quite homogeneous due to shear layer impingement upon the pantograph. The trailing edge region does not show important pressure coefficient values and their levels are close to those of the first study. Finally, coherences between w.p.f. and velocity fluctuations downstream from the trailing edge (not represented) indicate low levels of coherence (37% against 55% in the first study) because the velocity fluctuations are due both to the pantograph wakes and the downstream shear layer.

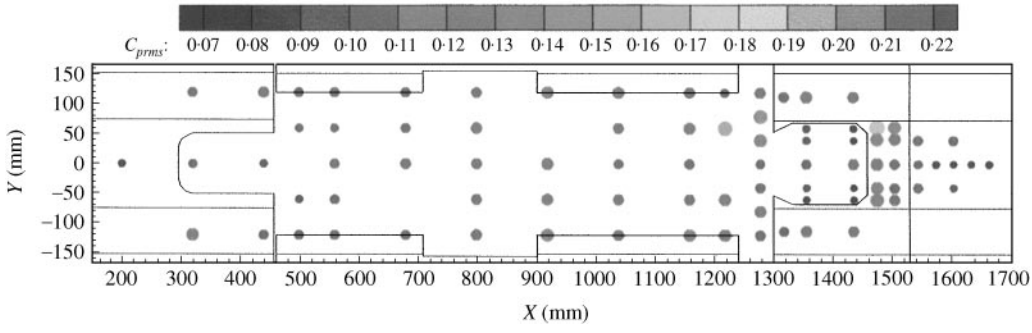

Figure 14. Root-mean-square pressure coefficients ($C_{P_{r.m.s}}$) with pantographs (not represented for clarity).

5. CONCLUSION

The two different studies show the rear vertical face being the most complex and turbulent region and the origin of the most important noise generation. An interesting point concerns the downstream flow structure (above the basin) which did not change for the different recess configurations. Coherence between velocities and wall pressure fluctuations indicate the low-frequency aspect and the dependence of the wall pressure fluctuations upon the turbulence restricted to a volume located close to the microphone. The addition of fences to the upstream hood has moved the reattachment point inside the recess downstream, increased the upstream shear layer turbulence, decreased the downstream shear layer turbulence and decreased the broadband noise level. The pantographs have increased the broadband noise level and decreased the downstream coherence by disturbing the flow, but have also generated discrete frequency peaks corresponding to the vortex shedding of the bow.

It can be concluded that the pantograph recess behaviour is different from that for usual rectangular cavities. The pantograph recess does not show any oscillation (acoustic or aerodynamic) for the different speeds tested, although local peaks exist due to both hood resonances and basin modes.

Finally, solutions to reduce the radiated noise can mainly be achieved either by modifying the cavity geometry with passive devices (spoiler, ramp [5, 8, 12, 15]) or by active control (mass injection [13]).

REFERENCES

1. A. J. Bilanin and E. E. Covert 1973 *AIAA Journal* **11**, 347–351. Estimation of possible excitation frequencies for shallow rectangular cavities.
2. H. H. Heller and D. Bliss 1976 *AIAA Paper* 75-491, *Progress in Astronautics and Aeronautics* **45**, 281–296. The physical mechanism of flow induced pressure fluctuation in cavities and concepts for their suppression.
3. C. K. W. Tam and P. J. W. Block 1978 *Journal of Fluid Mechanics* **89**, 373–399. On the stones and pressure oscillations induced by flow over rectangular cavities.
4. A. F. Charwat, F. C. Dewey, Jr, J. N. Roos and J. A. Hitz 1961 *Journal of Aerospace Sciences* **28**, 513–527. An investigation of separated flows. Part 2: flow in cavity and heat transfer.

5. M. E. Franke and D. L. Carr 1975 *AIAA Paper* 75-492. Effect of geometry on open cavity flow-induced pressure oscillations.
6. V. Sarohia 1977 *AIAA Journal* **15**, 984–991. Experimental investigation of oscillations in flows over shallow cavities.
7. D. Rockwell and E. Naudascher 1978 *Journal of Fluids Engineering* **100**, 152–165. Review: self-sustaining oscillations of flow past cavities.
8. L. L. Shaw 1979 *Journal of the Acoustical Society of America* **66**, 880–884. Suppression of aerodynamically induced cavity pressure oscillations.
9. L. S. Langston and M. T. Boyle 1982 *Journal of Fluid Mechanics* **125**, 53–57. A new surface-streamline flow-visualisation technique.
10. J. C. Hardin and D. S. Pope 1995 *AIAA Journal* **33**, 407–412. Sound generation by flow over a two-dimensional cavity.
11. J. M. Mendoza and K. K. Ahuja 1995 *Proceedings CEAS/AIAA-95*, 403–409. The effect of width on cavity noise.
12. O. Baysal, G. W. Yen and R. Fouladi 1994 *Journal of Vibration and Acoustics* **116**, 105–112. Navier–Stokes computation of cavity aeroacoustics with suppression devices.
13. A. Vakili and C. Gauthier 1994 *Journal of Aircraft* **31**, 169–174. Control of cavity flow by upstream mass-injection.
14. C. Noger, J. C. Patrat, J. Peube and J. L. Peube 1998 *ref.* 1*P*8*U*10*T*1.*DA*. First wind-tunnel campaign measurements: pantograph recess exploration and qualification.
15. N. M. Komerath, K. K. Ahuja and F. W. Chambers 1987 *AIAA Paper* 87-0166. Prediction and measurement of flows over cavities—a survey.